ARTICLES

Vibrational and XRD Study of the System $CdWO_4$−$CdMoO_4$

Marco Daturi,[†,‡] Guido Busca,*[,‡] Marie Madeleine Borel,[†] André Leclaire,[†] and Paolo Piaggio[§]

Laboratoire CRISMAT, ISMRA et Université de Caen, 6 Boulevard du Maréchal Juin, F-14050 Caen Cedex, France, Istituto di Chimica, Facoltà di Ingegneria, Università di Genova, P.le J. F. Kennedy, I-16129-Genova, Italy, and Dipartimento di Chimica e Chimica Industriale, Università di Genova, via Dodecaneso 31, I-16146 Genova, Italy

Received: September 30, 1996; In Final Form: December 8, 1996[⊗]

Mixed oxide powders belonging to the system $CdMo_xW_{1-x}O_4$ have been prepared by a hydrothermal method. They have been characterized by the Rietveld analysis of their XRD patterns and by IR and Raman skeletal spectroscopies. Virtually pure wolframite-type structures have been obtained for $x \leq 0.25$ and virtually pure scheelite-type structures have been obtained for $x \geq 0.75$. The vibrational spectra of both phases have been interpreted on the basis of the correlation method. In both solid solutions the Raman peaks due to the stretching modes of "terminal" W,Mo−O bonds split, while the corresponding IR bands shift significantly. The effect of the nature of tungsten coordination on the vibrational spectra is briefly discussed in relation to the use of vibrational spectroscopies to determine the structure of the surface species in supported tungsten oxide catalysts.

Introduction

Metal molybdates and tungstates represent a very relevant class of inorganic phases useful in the field of heterogeneous catalysis.[1−3] Molybdates and tungstates of relatively large bivalent cations (ionic radius ≥ 0.99 Å: Ca, Ba, Pb, Sr) crystallize in the so-called scheelite structure (scheelite = $CaWO_4$), where molybdenum or tungsten exhibit a tetrahedral coordination.[4] Scheelite-type tungstates and molybdates of the same divalent metal are reciprocally soluble in the entire compositional range.[5−7] Alternatively, tungstates and molybdates of smaller bivalent cations (ionic radius ≤ 0.77 Å: Fe, Mn, Co, Ni, Mg, Zn) can take the wolframite structure (wolframite = (Fe,Mn)WO_4), where tungsten and molybdenum exhibit an overall 6-fold coordination. Cd^{2+} compounds sit on the borderline ($r = 0.97$ Å, for the octahedral coordination) so that the molybdate takes the scheelite structure while the tungstate takes the wolframite structure.

The Scheelite-type mixed oxides have been the object of vibrational spectroscopic studies, based both on single crystals[8] and on powders,[6−7,9−11] that allowed a complete assignment of the IR bands and of the Raman peaks. Also solid solutions of scheelite-type molybdates and tungstates have been the object of vibrational studies.[7] In contrast, the detailed interpretation of the vibrational spectra of wolframite-type $M^{II}WO_4$ tungstates has not been attempted, to our knowledge. A partial band assignment has been proposed several years ago for some compounds, including $CdWO_4$, by Blasse,[12] based on the assumption that although the overall coordination at tungsten is six, a tetrahedral coordination can be taken as a good approximation, because two W−O bonds are very long. Recently, a detailed vibrational study of $M^IM^{III}(WO_4)_2$ mixed tungstates with a wolframite-like structure has been published.[13]

The vibrational spectra of these compounds, both scheelites and wolframites, have been recently taken into account in relation to their phase transformations at higher pressures.[14,15] Moreover, these compounds can be taken as "models" for surface species in oxides−supported-oxide catalysts.[16] In fact, molybdate and wolframate species are formed at the surface of oxide-supported molybdena and tungsta catalysts. Such monolayers escape XRD analysis, so that their structures must be investigated by other techniques such as IR, Raman, EXAFS, and other spectroscopies, in comparison with compounds with known structure.

Recently, the structure and the catalytic behavior of solid solutions in the system $CdMoO_4$−$CdWO_4$ have been investigated, based on both single crystals and powders.[17] In the present paper the results of a vibrational study of powders belonging to this system are reported.

Experimental Section

(a) Powder Preparation. The powder samples $CdMo_xW_{1-x}O_4$, with $x = 0$, 0.125, 0.25, 0.5, 0.75, 1, were prepared via hydrothermal synthesis in a Teflon-lined autoclave, adding 2 cm^3 of water and the 5% in weight of a salt such as NaF, KF, and KCl to the stoichiometric mixture of the oxide precursors: CdO (UCB, for analysis), MoO_3 (Prolabo, 99%), WO_3 (Hermann C. Starck, 99%). The temperature cycle consisted in a heating ramp of 50 K/h, an isothermal heating at 473 K for 48 h, a cooling rate of 1 K/h until 423 K, and a final cooling rate to room temperature, at a speed of 3 K/h.

(b) Characterization Techniques. The patterns of the samples have been collected with a Philips 1701 X-ray powder diffractometer (Cu Kα radiation, Ni filter, 45 kV, 35 mA). Structural calculations have been performed by the Rietveld-type profile refinement computer program FULLPROF.[18] The relevant parameters are summarized in Table 1.

The IR and FIR spectra were recorded by a Nicolet Magna 750 Fourier transform instrument. The FT-Raman spectra were recorded using a Brucker FTS100 (Nd:YAG laser). The skeletal spectra in the region above 400 cm^{-1} have been recorded with

[†] ISMRA et Université de Caen.
[‡] Instituto di Chimica.
[§] Dipartimento di Chimica e Chimica Industriale.
[⊗] Abstract published in *Advance ACS Abstracts,* March 15, 1997.

S1089-5647(96)03008-8 CCC: $14.00

TABLE 1: Rietveld Main Parameters of the Refined Structures

atom	position	*x*	*y*	*z*	*B* (Å^2)	occupancy	agreement factors
			$CdWO_4$, S.G. *P*2/*c*				
W	2e	0	0.25	0.1784(3)	0.24(4)	0.5	$R^a = 5.36\%$
Cd	2f	0.5	0.75	0.3020(5)	0.46(9)	0.5	$R_p = 7.34\%$
O1	4g	0.189(2)	0.454(3)	0.901(2)	1	1	$R_{wp} = 11.1\%$
O2	4g	0.250(2)	0.393(3)	0.360(2)	1	1	$\chi^2 = 4.23\%$
			$CdMoO_4$, S.G. $I4_1/a$				
							$R = 6.71\%$,
Mo	4a	0	0.25	0.125	0.41(3)	0.25	$R_p = 12.9\%$
Cd	4b	0	0.25	0.625	0.10(3)	0.25	$R_{wp} = 19.2\%$
O	16f	0.240(2)	0.091(2)	0.0421(9)	1	1	$\chi^2 = 5.96\%$
			$CdMo_{0.25}W_{0.75}O_4$, S.G. *P*2/*c*				
W	2e	0	0.25	0.1760(7)	0.62(1)	0.375	$R = 4.83\%$
Mo	2e	0	0.25	0.1760(7)	0.62(1)	0.125	$R_p = 8.71\%$
Cd	2f	0.5	0.75	0.2991(9)	0.5	0.5	$R_{wp} = 11.7\%$
O1	4g	0.181(4)	0.443(7)	0.919(4)	1	1	$\chi^2 = 2.31\%$
O2	4g	0.240(4)	0.416(8)	0.381(4)	1	1	
			$CdMo_{0.75}W_{0.25}O_4$ S.G. $I4_1/a$				
Mo	4a	0	0.25	0.125	0.68(2)	0.1875	$R = 3.95\%$
W	4a	0	0.25	0.125	0.68(2)	0.0625	$R_p = 10.9\%$
Cd	4b	0	0.25	0.625	0.55(1)	0.25	$R_{wp} = 15.4\%$
O	16f	0.242(3)	−0.592(2)	0.042(1)	1	1	$\chi^2 = 5.46\%$

[a] Bragg factor.

TABLE 2: Phase Composition of the Powders under Study

	XRD Rietveld analysis					
		unit cell parameters				
composition	main phase	*a* (Å)	*b* (Å)	*c* (Å)	γ (deg)	impurities
$CdWO_4$	wolframite	5.026(1)	5.078(1)	5.867(1)	91.47(1)	
$CdMo_{0.125}W_{0.875}O_4$	wolframite	5.031(1)	5.071(2)	5.857(2)	91.44(3)	
$CdMo_{0.25}W_{0.75}O_4$	wolframite	5.031(1)	5.074(1)	5.858(1)	91.48(2)	scheelite traces
$CdMo_{0.5}W_{0.5}O_4$	wolframite 60%	5.029(1)	5.072(1)	5.858(1)	91.48(1)	
	scheelite 40%	5.164(1)		11.171(1)		
$CdMo_{0.75}W_{0.25}O_4$	scheelite	5.158(1)		11.187(1)		WO_3 and wolframite traces
$CdMoO_4$	scheelite	5.156(1)		11.196(1)		

TABLE 3: Interatomic Distances (Å) and Bond Angles (deg) in $CdMoO_4$ and $CdWO_4$, As Determined by the Rietveld Analysis of the Powder XRD Patterns

$CdMoO_4$ (scheelite-type structure) polyhedra				$CdWO_4$ (Wolframite-type structure) polyhedra			
MoO_4	Mo−O	distances	1.75(1) × 4	WO_6	W−O (I)	distances	1.78(1) × 2
	O−Mo−O	angles	116.0(4) × 2		W−O (II)		1.86(1) × 2
			106.3(4) × 4				2.13(1) × 2
CdO_8	Cd−O	distances	2.40(1) × 4		O(I)−W−O(I)	angles	107.3(5) × 1
			2.44(1) × 4		O(I)−W−O(II) sh*		96.4(5) × 2
	O−Cd−O	angles	69.1(3) × 4				101.1(6) × 2
			73.0(3) × 4		O(I)−W−O(II) l*		87.1(5) × 2
			76.3(3) × 4				161.7(5) × 2
			80.0(3) × 2		sh* O(II)−W−O(II) sh*		150.3(5) × 1
			98.6(3) × 4		l* O(II)−W−O(II) l*		81.4(5) × 1
			126.0(3) × 4		l* O(II)−W−O(II) sh*		88.1(5) × 2
			134.4(3) × 2				69.2(5) × 2
			152.4(3) × 4	CdO_6	Cd−O	distances	2.20(1) × 2
							2.25(1) × 2
							2.47(1) × 2
					O−Cd−O	angles	80.7−162.7

[a] sh = shorter W−O(II) bond. [b] l = longer W−O(II) bond.

KBr pressed disks and with a KBr beam splitter, while those in the far infrared region (400−50 cm^{-1}) have been recorded using the powder deposited on polyethylene disks and with a "solid substrate" beam splitter.

Results and Discussion

(a) Pure End-Member Compounds $CdWO_4$ and $CdMoO_4$: X-ray Diffraction Study. The phase compositions of the samples on which the present paper will be focused, as determined by the Rietveld analysis of the experimental powder XRD patterns, are summarized in Table 2.

In Figure 1 the experimental and simulated XRD patterns for the compounds $CdWO_4$ (wolframite-type structure) and $CdMoO_4$ (scheelite-type structure) are reported. The interatomic distances and the bond angles in these compounds, as determined by the Rietveld analysis, are reported in Table 3.

In the wolframite structure of $CdWO_4$ (space group $P2/c \equiv C_{2h}^4 \equiv$ no. 13, $Z = 2$) the overall coordination around tungsten is six, giving rise to ribbons of edge-sharing distorted octahedra, which form a polymeric anionic structure with composition $[(W_2O_8)^{4-}]_n$, as shown in Figure 2. Similarly, the coordination at cadmium is also six and gives rise to parallel ribbons of edge-

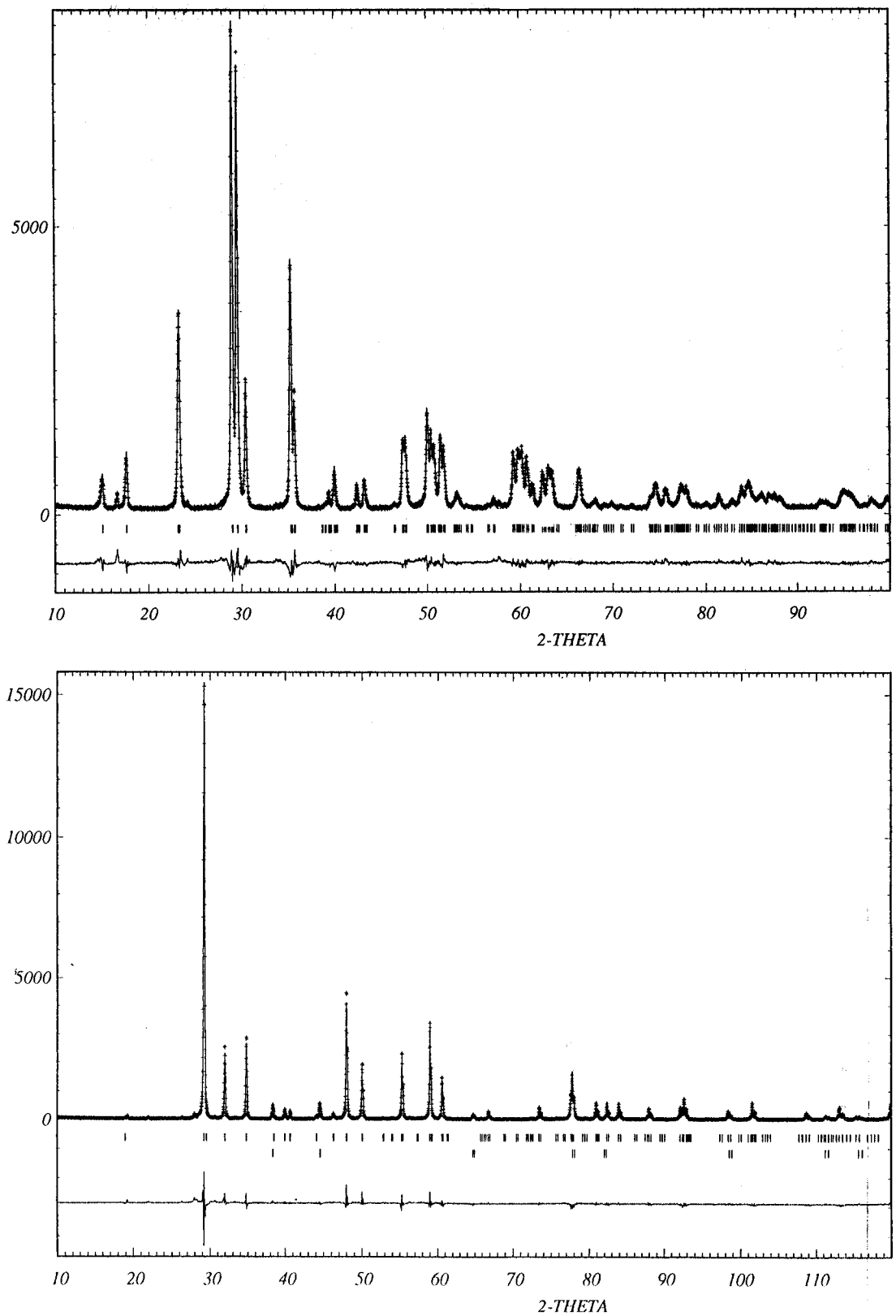

Figure 1. Experimental (+), calculated (−), and difference XRD patterns, for the "pure" mixed oxide samples $CdWO_4$ (a, top) and $CdMoO_4$ (b, bottom). The secondary phase in the b plot belongs to the sample holder.

sharing distorted octahedra. In fact, the wolframite structure can be taken as a slightly distorted superstructure of the α-PbO_2-type structure, where the octahedra are occupied alternatively by the two different cations.[4]

Two types of oxygen atoms, both located in C_1 symmetry sites, are distinguished. O(I) are bonded with one short bond (1.782 Å) to one tungsten atom (giving rise to a "terminal" W−O bond) and to two Cd ions with two relatively long bonds (2.417 and 2.273 Å). O(II) bridges two W atoms with longer bonds (1.909 and 2.146 Å) and also interacts, with a relatively short bond, with one Cd atom (2.199 Å).

However, the W−O−W couples of bridges are very asymmetric, two tungsten−oxygen distances being definitely longer than the other four around any W atom, so that it seems

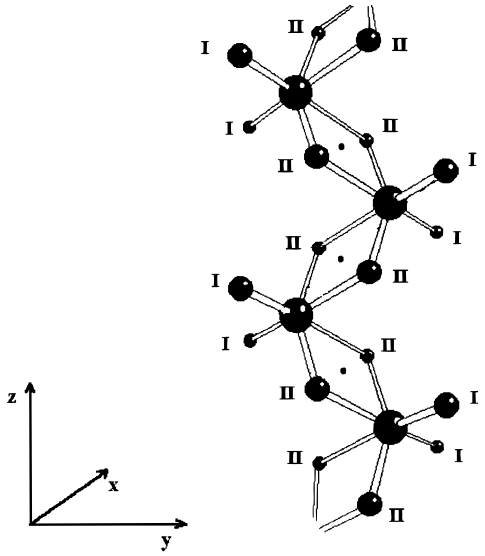

Figure 2. View of the structure of the polymeric $[(W_2O_8)^{4-}]_n$ anion in the wolframite structure of $CdWO_4$. Bridging and terminal oxygens are distinct; the dots (•) indicate inversion centers.

reasonable to interpret this structure on the basis of a distorted tetrahedral coordination around tungsten, as proposed by Blasse.[12] The validity of such an approximation will be checked below on the basis of vibrational spectroscopies.

On the contrary, the $CdMoO_4$ belongs to the Scheelite-type structure (space group $I4_1/a \equiv C_{4h}^6 \equiv$ no. 88, $Z = 4$); the coordination around molybdenum is quite symmetrically tetrahedral, like for any scheelite-type compound, while the overall coordination of cadmium is eight. All oxygen atoms are equivalent and linked to one Mo atom with a short "terminal" bond and to two Cd ions with a slightly asymmetric bridge.

The structures determined here correspond to those previously reported for $CdWO_4$[19] and for $CdMoO_4$.[20]

(b) Wolframite-Type $CdWO_4$: Vibrational Study. The IR and Raman spectra of the $CdWO_4$ powder are reported in Figures 3a and 4a, respectively. In Table 4 the number of total modes is determined, on the basis of the so-called correlation method.[21] The number of well-resolved peaks in our Raman spectrum, 18, corresponds to the number of the expected Raman active modes. Similarly, the number of maxima in our IR spectrum is closely similar to the number of expected IR active modes, 15.

In Tables 5 and 6 the expected vibrational modes for $CdWO_4$ are identified on the basis of two different models. In both cases we separate the "internal" vibrational modes associated with the $[(W_2O_8)^{4-}]_n$ polymeric anion from those associated with Cd−O bonds and lattice vibrations. This is reasonable because of the strongly different electronegativity of hexavalent tungsten with respect to that of divalent cadmium that would result in highly covalent W−O bonds and in more ionic Cd−O bonds.[22] In Table 5, we assume O(I) to be terminally linked to one tungsten atom (in fact they are also linked with two Cd atoms), giving rise to short WO_2 entities, and we separate the vibrations of the WO_2 groups from those of the longer W−O(II) bonds that give rise to ribbons with $[W_2O_4]_n$ composition. In Table 6 an alternative assignment is proposed, based on a tetrahedral coordination around tungsten, as previously done by Blasse.[12] This is made by artificially "breaking" the longest W−O(II) bond interactions, so that isolated WO_4 units with highly distorted tetrahedral symmetry are formed. In fact, four of the six W−O bonds surrounding every tungsten atom are relatively short (below 2 Å), while the other two are definitely longer (2.15 Å). In Table 7 the observed bands are assigned, on the basis of the model of Table 5, i.e. on the overall coordination six of tungsten, because this appeared to be more appropriate, as discussed below.

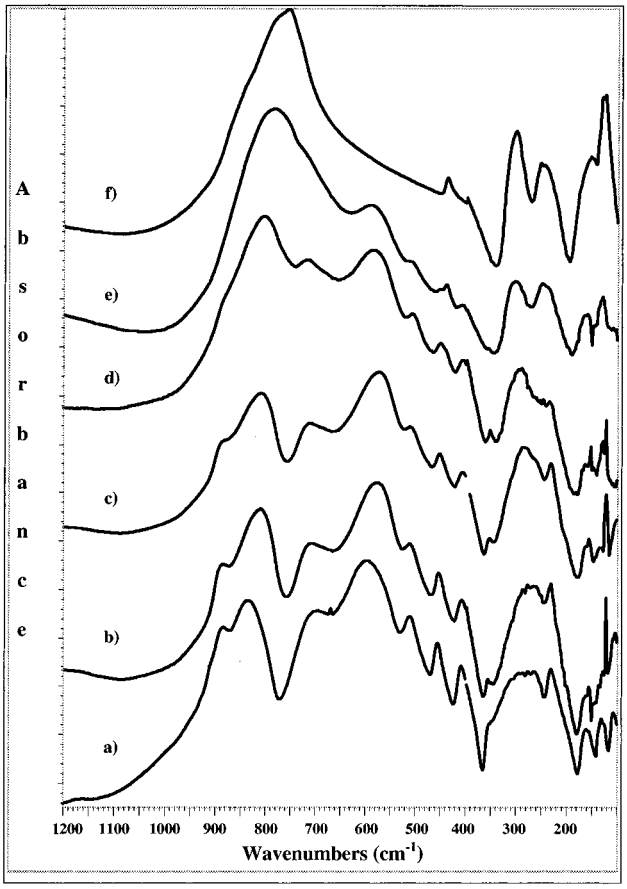

Figure 3. FT-IR spectra of $CdMo_xW_{1-x}O_4$ powders: $x = 0$ (a), $x = 0.125$ (b), $x = 0.25$ (c), $x = 0.5$ (d), $x = 0.75$ (e), $x = 1$ (f).

In the region 1000−750 cm^{-1}, two maxima are found both in IR and in Raman spectrum. The highest frequency component is more intense in Raman, while the reverse is true for IR. The peak at 897 cm^{-1} is the strongest in the overall Raman spectrum. This frequency region is typical for stretchings of short terminal W−O bonds. We can consequently assign with confidence the strongest Raman peak to the "totally symmetric" stretching mode of the four shortest wolframyl bonds in the unit cell. This mode almost coincides in its frequency to the highest frequency IR mode, which is relatively weak, and must be assigned to the asymmetric component (with respect to the center of symmetry) of the ν_{sym} WO_2 mode of the same terminal wolframyls. The more intense IR peak in this region must be assigned to the IR active ν_{as} WO_2 component (asymmetric with respect to the center of symmetry), while the corresponding Raman active mode (symmetric with respect to the center of symmetry) is reasonably identified as responsible for the weaker Raman peak at 771 cm^{-1}.

The bands in the region 750−500 cm^{-1} can be assigned to stretching modes of the longer W−O bonds, i.e. of the W_2O_2 parallelograms involved in the W_2O_4 polymeric chain. In this region we observe four Raman peaks and two IR peaks, as expected on the basis of a 6-fold coordination of tungsten. We can assign the four higher frequency modes (706 and 687 cm^{-1} in Raman, 695 and 595 cm^{-1} in IR) to the modes arising from the asymmetric stretching of the W−O−W bridges, while the two lower frequency Raman modes (546 and 514 cm^{-1}) can be assigned to the modes arising from the symmetric W−O−W stretching modes.

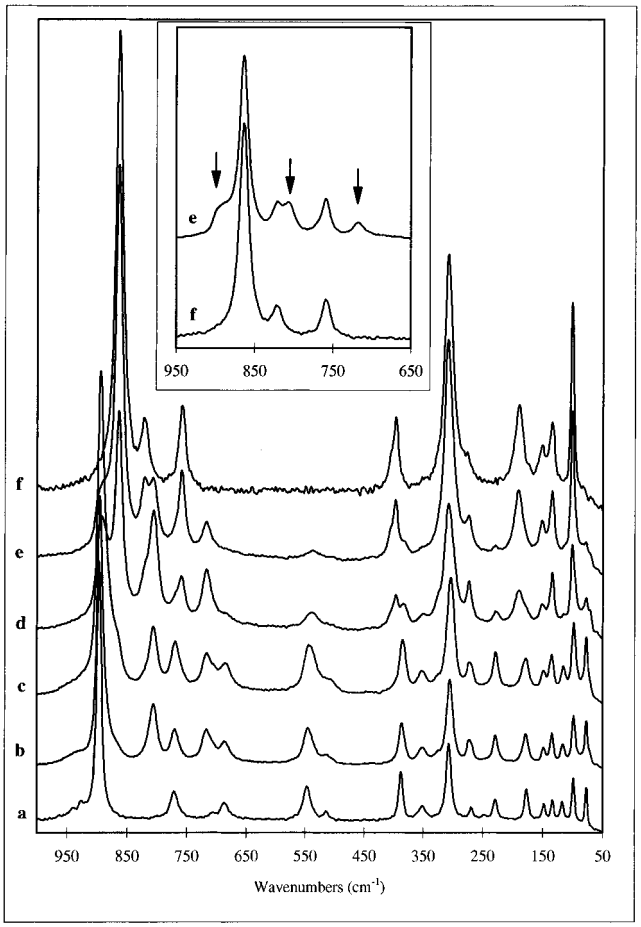

Figure 4. FT-Raman spectra of $CdMo_xW_{1-x}O_4$ powders: $x = 0$ (a), $x = 0.125$ (b), $x = 0.25$ (c), $x = 0.5$ (d), $x = 0.75$ (e), $x = 1$ (f). In the window, the splitting induced by W insertion in the scheelite structure is pointed out.

TABLE 4: Determination of the Total Modes for $CdWO_4$ (Space Group $P2/c \equiv C_{2h}^4 \equiv$ no. 13, $Z = 2$)

atom	Wickoff notation	site sym	
W	2e	C_2	$A_g + A_u + 2\,B_g + 2\,B_u$
Cd	2f	C_2	$A_g + A_u + 2\,B_g + 2\,B_u$
O (I)	4g	C_1	$3\,A_g + 3\,A_u + 3\,B_g + 3\,B_u$
O (II)	4g	C_1	$3\,A_g + 3\,A_u + 3\,B_g + 3\,B_u$

In the region 520−330 cm^{-1} we observe four other IR bands and two Raman peaks. Here we can find the in-plane deformation modes of the W−O bonds (both terminal and bridging). The additional modes arising from the symmetric in-plane deformation of W_2O_2 parallelograms involve motions of W atoms and consequently should be shifted at lower frequencies.

In the region 330−250 cm^{-1} we observe a rather strong Raman peak, with a weaker peak at lower frequency, and a broad IR absorption certainly constituted by more than one band. The quite strong Raman peak at 307 cm^{-1} can be assigned to the symmetric stretching of CdO_6 octahedra, and the other bands in this region can be assigned to the other modes associated with Cd−O stretchings.

Even more difficult is the assignment of the bands below 300 cm^{-1}, where out-of-plane W−O deformations are expected to be superimposed to lattice modes and the librational mode of the W_2O_8 polymeric anion. These modes are certainly strongly coupled.

The assignments proposed here and in Table 7 for the bands above 300 cm^{-1}, following the modes described in Table 5, seem quite satisfactory, in particular in relation with the position of the different modes in IR and in Raman spectra and their relative intensities. We note that all the most intense Raman peaks can be assigned as belonging to A_g symmetry.

As already said, we have alternatively tried to interpret the spectra on the basis of a tetrahedral coordination of tungsten. Accordingly, the four intense IR bands we observe in the region above 550 cm^{-1}, one of which (that at highest frequency) is the weakest, could in principle be due to the four IR active stretching modes of the two $[WO_4]^{2-}$ tetrahedra in the unit cell.

However, looking at the Raman pattern, this model is unsatisfactory. In fact, we observe six Raman modes above 500 cm^{-1}, only four of which can be assigned to stretchings of WO_4 tetrahedra. On the other hand, bands in this wavenumber range can be due neither to deformation modes of WO_4 ions nor to Cd−O stretchings or lattice modes. In effect, the remaining Raman peaks at 547 and 514 cm^{-1} are just the stretchings of the longest W−O bonds we have "artificially broken" in the "tetrahedral model" of Table 6. In other words, we have two stretching modes in excess, which allow us to rule out the possibility of assigning the spectrum of $CdWO_4$ on the basis of a tetrahedral coordination at tungsten.

The IR and Raman spectra can be compared with those reported in the literature by different authors. The agreement of our data with those of Blasse[12] and Jarayaman et al.[15] is very good, while in the IR spectrum of Brown et al.[10] several peaks are apparently lacking. The spectra of $CdWO_4$ show relevant similarities to those of $M^{I}M^{III}(WO_4)_2$ mixed tungstate with a wolframite-like structure, reported recently by Hanuza et al.[13] However, the interpretation we propose here does not completely agree with that proposed by these authors and is by far more detailed.

Daniel et al.[23] proposed a correlation between the force constant and length for W−O bonds, in tungstate compounds. According to these authors, the correlation curve coincides with that proposed previously by Cotton and Wing[24] for Mo−O bonds in molybdate compounds. In Figure 5 these correlations are represented. We added in that picture also the data concerning the W−O "terminal" bonds in $CdWO_4$. To do this, we calculated the force constant as done by Cotton and Wing,[24] using for ν_{sym} and ν_{as} the average of their IR and Raman active components (Table 7). This point agrees with the correlation quite well.

(c) Scheelite-Type $CdMoO_4$: Vibrational Study. The interpretation of the spectrum of $CdMoO_4$ takes advantage of the many previous vibrational studies on scheelite-type compounds,[6−11] including a single-crystal vibrational study.[8] The determination of the total modes (Table 8), the identification of the different optical modes (Table 9), and the assignment proposed in Table 10 agree with those previous given by Liegeois-Duyckaerts and Tarte[6,7] and with the symmetries deduced from the reflection single-crystal measurements of Barker.[8]

We calculated the force constant for Mo−O stretching as done by Cotton and Wing,[24] but using for the symmetric stretching mode the wavenumber of its Raman active component, the other component being both IR and Raman inactive. For the asymmetric stretching we averaged the wavenumbers of the two coincident IR active modes and of the two Raman active modes. Also this point agrees with the correlation, reported in Figure 5.

(d) $CdW_{1-x}Mo_xO_4$ Mixed Compounds: XRD Characterization of the Solid Solutions. As already said, we observe the formation of virtually pure monophasic wolframite-type phases of $CdW_{1-x}Mo_xO_4$ mixed compounds for $x \leq 0.25$ (see the experimental and calculated XRD patterns in Figure 6a, for

TABLE 5: Determination and Assignments of the Vibrational Modes of $CdWO_4$[a]

		$[(W_2O_8)^{4-}]_n$																
		internal vibrations																
		2 × WO_2 terminal							$[W_2O_4]_n$ chain									
sym	act	ν_{as}	ν_{sym}	δ	r	t	w	tot	ν_{as}	ν_{sym}	δ_{sym}	δ_{as}	r	tot	rot	2 Cd^{2+} lattice	vibr	acoust	tot
A_g	R	1	1	1				3	1	1	1		1	4		1	8		8
A_u	IR				1	1	1	3	1			1	1	3		1	7	1	8
B_g	R				1	1	1	3	1	1	1		1	4	1	2	10		10
B_u	IR	1	1	1				3	1			1	1	3		2	8	2	10
totals		2	2	2	2	2	2	12	4	2	2	2	4	14					
		26													1	6	33	3	36

[a] rot = rotation; ν = stretching; δ = in-plane deformation; r = rocking; t = twisting; w = wagging.

TABLE 6: Determination and Assignments of the Vibrational Modes of $CdWO_4$, Based on a Hypothetical Tetrahedral Coordination at Tungsten

		2 × $(WO_4)^{2-}$									
		internal				external					
sym	act	ν_{sym}	ν_{as}	δ_{ip}	δ_{oop}	rotations	translations	2 Cd^{2+}	vibr	acoust	tot
A_g	R	1	1	2	1	1	1	1	8		8
A_u	IR	1	1	2	1	1		1	7	1	8
B_g	R		2		2	2	2	2	10		10
B_u	IR		2		2	2		2	8	2	10
totals		2	6	4	6						
		18				6	3	6	33	3	36

TABLE 7: Assignments of the Observed Spectra of $CdWO_4$ and of the Wolframite-Type $CdMo_xW_{1-x}O_4$ Solid Solutions

						$CdMo_xW_{1-x}O_4$					
$CdWO_4$						$x = 0.125$		$x = 0.25$		x = 0.5[a]	MoO_2
R	IR	sym	WO_2 terminal	$[W_2O_4]_n$ chain	other	R	IR	R	IR	R	terminal
896		A_g	ν_{sym}			896		894		892	
						806		806		807	ν_{sym}
	884	B_u					884		883		
	835	B_u	ν_{as}				809		809		
771		A_g				770		769			
						717		716			ν_{as}
706		B_g				706 sh		706 sh			
687		A_g		ν_{as}		687		686		685	
	693	A_u					707		710		
	595	B_u					576		573		
547		A_g		ν_{sym}		545		544		538	
514		B_g				513		512			
	510	B_u		δ_{as}			510		510		
	455	A_u					453		451		
	408	B_u	δ				407		405		
387		A_g				386		385			
	354	A_u	r				354		352		
351		B_g				351		353			
307		A_g				306		304			
	310−260				ν(Cd−O)		300−260		286		
269						273		272			
248											
229	230					229	232	229	231		
177						178	165	178	164		
148	161				out-of-plane modes	149	156	149	155		
133	131				and lattice modes	134		135			
117	107					116	121	116	122	115	
99						98	105	98	96		
77						77		77			

[a] Biphasic sample.

$x = 0.25$), while virtually pure monophasic scheelite-type phases are observed for $x \geq 0.75$ (see the experimental and calculated XRD patterns in Figure 6b, for $x = 0.75$), using the present preparation method. In the previous work,[17] pure monophasic scheelite-type phases in both powder and single crystal form were prepared with x as high as 0.5. In Table 2, the unit cell parameters and volume of the scheelite-type and of the wolframite-type solid solution powders investigated here are reported. It is evident that the unit cell volume of both phases is almost unaffected by forming solid solution. However, in the case of the wolframite-type structures while the *a* parameter tend to increase by substitution, the *b* and *c* parameters tend to decrease. This points to a deformation of the coordination polyhedra around W,Mo and around Cd, evidenced also by the small but significant modifications of the bond lengths and angles, as shown in detail in Table 11. In the case of the scheelite-type structure the *c* parameter decreases significantly by W for Mo substitution, while *a* tends to increase.

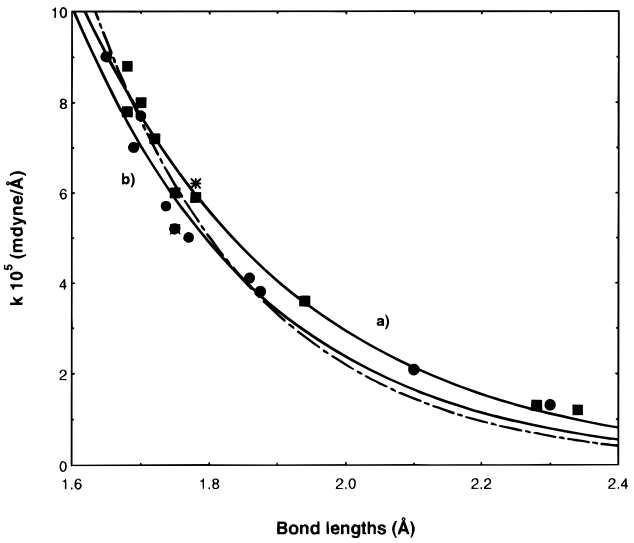

Figure 5. Plot of the Mo−O and W−O bond stretching constants versus bond lengths: (■) values for molybdates from ref 23; (●) values for tungstates from ref 24; (*) data from this work. (a) Solid curve: fitting of data points of molybdates. (b) Solid curve: fitting of data points of tungstates. Dashed curve: Hardcastle and Wachs's relation for molybdates.[31]

TABLE 8: Determination of the Total Modes for $CdMoO_4$ (space group $I4_1/a \equiv C_{4h}^6 \equiv$ no. 88, $Z = 4$)

atom	Wickoff notation	site sym	
Mo	4a	S_4	$B_g + A_u + E_g + E_u$
Cd	4b	S_4	$B_g + A_u + E_g + E_u$
O(I)	16f	C_1	$3\,A_g + 3\,B_g + 3\,E_g + 3\,A_u + 3\,B_u + 3\,E_u$

The addition of molybdenum to $CdWO_4$ (wolframite-type) causes a slight increase of the W,Mo−O bond length and the partial decrease of the asymmetry of the W,Mo−O−W,Mo bridges. The former effect disagrees with the slightly higher ionic radius of octahedrally coordinated W^{6+} with respect to octahedral Mo^{6+} according to Shannon,[25] in contrast to the inverse trend previously proposed by Shannon and Prewitt.[26] However, the increase of the bond lengths can be compensated by the deformation of the 8-fold coordination sphere. The Cd−O distances slightly decrease in parallel. This distance, already shorter for $CdWO_4$ (average value 2.31 Å) than that measured in the binary compound Cd−O (ca. 2.35 Å), decreases to a very small value by adding molybdenum (2.26 Å). Actually, the observed differences lie within the limits of the 3σ reliability range, so that it is doubtful that they are significant. However, the repeatability of such measures on the different solid solution samples allows us to be confident of them and to suggest that the forced contraction of the Cd−O distances can be a reason for destabilizing the wolframite-type structure and, accordingly, to favor the alternative scheelite-type structure. As already mentioned, the wolframite structure can be taken as a slightly distorted superstructure of the α-PbO_2-type; in this case all the octahedra are occupied by the same cation, Pb^{2+}, while for wolframites two different cations occupy them, orderly, forming octahedra ribbons along the *z* axis. The excessive difference in the ionic radius of the two alternating cations in the wolframite-type structure is certainly a factor that tends to destabilize it. This structure is stable in the case of wolframates and tungstates only if the countercation is sufficiently small. Cd^{2+} is at the borderline. It is consequently reasonable to conclude that the substitution of the W^{6+} by the even smaller Mo^{6+} increases such a destabilization because it causes a further contraction of the CdO_6 octahedra and, above a limit, causes the collapse into the scheelite-type structure.

The substitution of Mo for tungsten in the scheelite-type phase causes a slight increase of the Mo,W−O distance too, in agreement with the greater ionic radius of tetrahedrally coordinated W^{6+} with respect to tetrahedral Mo^{6+} according again to Shannon.[25] On the other hand, the unit cell parameters are very weakly affected by this substitution. So, the Cd−O bond distances, measured to be anomalously long (see above), decrease to a value (2.38 Å) more similar to that of CdO (2.35 Å), and correspondingly, the dodecahedron around Cd becomes definitely more regular (all Cd−O distances become nearly equivalent). The measured Mo,W−O bond distances in the scheelite-type solid solutions (1.82 Å) are longer than the W−O distance in scheelite, $CaWO_4$ (1.79 Å), while the Cd−O distances are shorter than the Ca−O distances of scheelite (average value 2.46 Å).

(e) $CdW_{1-x}Mo_xO_4$ Mixed Compounds: Vibrational Study of the Solid Solutions. The IR spectra of the wolframite-type $CdW_{1-x}Mo_xO_4$ solid solutions (Figure 3b,c) present all and only the bands present on the pure compound $CdWO_4$, with no band splittings. However, some of the bands undergo significant shifts, as shown in Table 7. In particular, the IR active components of the asymmetric stretching mode of WO_2 terminal bonds and of the $[W_2O_4]_n$ chains both shift definitely at lower frequencies.

The Raman spectra of the wolframite-type $CdW_{1-x}Mo_xO_4$ solid solutions (Figure 4b,c) show a different behavior with respect to the IR spectra. In fact, splitting of the higher frequency Raman active modes occurs. In particular, the Raman active components of both the asymmetric and the symmetric stretching modes of the shorter WO_2 bonds split, with the appearance of new peaks at lower frequencies. In effect we can note that Mo−O stretchings are generally located at lower frequency than W−O stretchings in isostructural compounds. This is reported for the $[MoO_4]^{2-}$ and $[WO_4]^{2-}$ anions in water solution[27] and in scheelite-type compounds like Ca−molybdate and -tungstate,[6,7] as well as for single terminal Mo═O and W═O bonds on oxide surfaces.[16,28] This is despite the fact that the force constants are, for the same bond distance, greater for molybdates than tungstates. As a conclusion, this means that the W−O bond lengths are generally longer than Mo−O bond lengths in isostructural compounds, in agreement with their relative crystal radii.[25]

Interestingly, the position of the main Raman peaks associated with W−O stretchings is not modified by Mo addition. Moreover, all deformation and lattice modes are also apparently insensitive to Mo addition.

The splittings observed in Raman spectroscopies, with the formation of components at lower frequencies, and the shifts to lower frequencies of the IR bands, in the wolframite-type $CdW_{1-x}Mo_xO_4$ solid solutions by increasing *x* agree with each other and parallel the slight increase of the metal-to-oxygen bond lengths (Table 11). The compression of the O−Mo,W−O angle appears to be more significant. This is likely due to the higher electronegativity of tungsten with respect to Mo and to the resulting higher covalence of the W−O bond with respect to the Mo−O bond.[22] In effect, the "microscopic" nature of Raman scattering (and, more in general, of vibrational spectroscopies) allows one to distinguish between Mo and W randomly distributed in the wolframite structure, unlike XRD. This is due to the longer dimensional range associated with diffraction phenomena, averaging the Mo,W−O distances. Some of us emphasized recently the role of Raman spectroscopies in refining the structural data arising from XRD in other oxide systems.[29,30]

TABLE 9: Determination and Assignments of the Vibrational Modes in $CdMoO_4$

		2 × MoO_4									
		internal				external					
sym	act	ν_{sym}	ν_{as}	δ_{ip}	δ_{oop}	rotations	translations	2 Cd^{2+}	total	vibr	acoust
A_g	R	1		1		1			3	3	
B_g	R		1	1	1		1	1	5	5	
E_g	R		1		1	1	1	1	5	5	
A_u	IR		1	1	1		1	1	5	4	1
B_u		1		1		1			3	3	
E_u	IR		1		1	1	1	1	5	4	1
total dof[a]		2	6	4	6	6	6	6	36	33	3
		18									

[a] dof = degrees of freedom.

TABLE 10: Assignments of the Observed Spectra of $CdMoO_4$ and of the Scheelite-Type $CdMo_xW_{1-x}O_4$ Solid Solutions

wavenumber (cm^{-1})													
$CaMoO_4$													
single crystal (ref 8)		powder (ref 6, 7)		$CdMoO_4$ powder (t.w.)		$CdMo_{0.75}W_{0.25}O_4$ powder (t.w.)		$CdMo_{0.5}W_{0.5}O_4$ powder (t.w.)				MoO_4[d]	WO_4[d]
IR LO	IR TO	IR	R	R	IR	R	IR	R	sym				
						895		891[b]	A_g	ν_{sym}	W−O		931
			879	863		864		862			Mo−O	897	
			848	822		825		821[c]			Mo−O	837	838
						807		806[b]			W−O		
			794	759		758		759	$B_{g,Eg}$	ν_{as}	Mo−O		
						717		717[b]			W−O		
913	802						782		$A_{u,Eu}$		W−O, Mo−O		
897	775	813			752						Mo−O		
434	425	431			435 (400)		437 (406)		A_u		δ_{ip}		
			403	402		402		404[c]	$B_{g,Eg}$		δ_{oop}		
			392	396		397		396			δ_{oop}		
358	318	329			300		309		E_u		δ_{oop}	317	325
			323	308		309		308[b]	A_g		δ_{ip}		
			268	277		274		273	B_g		δ_{ip}		
319	245	284			250		248		A_u		δ_{oop}		
261	208	237											
						229							
			205	189		191		189		ν(Cd−O) and translations MoO_4			
			191	173									
197	196	200			152		159						
			144	150		151		151[b]					
			112	135		134		134[b]					
156	150	153			125		129						
				(105)						librational modes			
			83	101		101		101[b]	A_g				

[a] Biphasic samples. [b] Peaks (partly) superimposed to those of the wolframite-type solid solution. [c] Peaks evident as shoulders. [d] Spectral features for tetrahedral ions in solution (ref 23).

We can attempt to use the correlation between the force constants and the lengths for W−O bonds, reported in Figure 5 and assumed, according to Daniel et al.,[23] to coincide with that proposed by Cotton and Wing[24] for Mo−O bonds, to have data on the geometry of the molybdate species in the wolframite-type solid solutions. To calculate the Mo−O bond distances we have to know the O−Mo−O bond angle, or vice versa. However, using the approximate secular equation as done by Cotton and Wing,[24] we concluded that the splitting of the stretching mode is more sensitive to the stretch−stretch interaction constant than to the O−M−O value.

The IR spectrum of the scheelite-type $CdW_{1-x}Mo_xO_4$ solid solution (Figure 3e) presents some definite differences with respect to that of $CdMoO_4$ (Figure 3f). The main maximum, assigned to the asymmetric stretching mode of the MoO_4 tetrahedra, shifts to higher frequency near 30 cm^{-1} by adding W, again in agreement with the stronger W−O bond. Moreover, a new, broad component appears, near 590 cm^{-1}.

The Raman spectrum of the scheelite-type $CdW_{1-x}Mo_xO_4$ solid solution (Figure 4e) shows three additional strong components with respect to that of $CdMoO_4$ (Figure 4f). These features can be interpreted as due to splittings of the highest frequency Mo−O stretchings, according to the appearance of W−O stretching modes. Interestingly, the Raman active component of the symmetric stretching mode of the tetrahedra (the other component is both Raman and infrared inactive, see Table 10) shifts up, as usual for W to Mo substitution. On the contrary, the Raman active components of the asymmetric stretching of the tetrahedra shift down, in contrast to the IR active modes (supposed to be superimposed) that shift upward. This implies a modification in the internal couplings, likely associated with a deformation of the bond angles.

From the data we have and the correlation reported in Figure 5 (see below) we can calculate that the W−O distance in the scheelite-type solid solution is 1.796 Å, which compares well with the W−O distance in $CaWO_4$, reported to be 1.79 Å, but apparently disagrees with the value deduced from the Rietveld

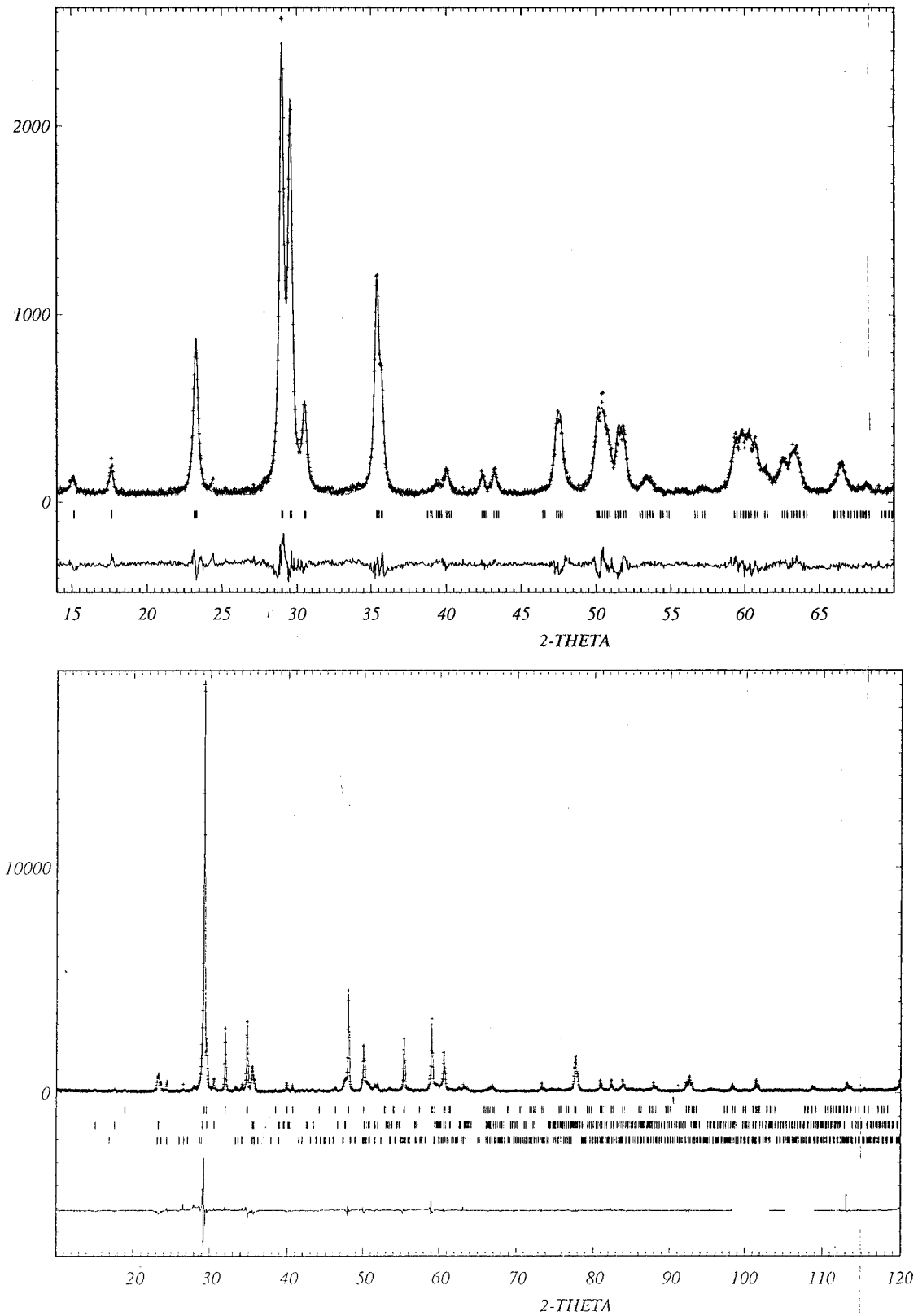

Figure 6. Experimental (+), calculated (—), and difference XRD patterns, for the "pure" solid solutions: (a, top) wolframite-type $Cd(Mo_{0.25}W_{0.75})O_4$ and (b, bottom) scheelite-type $Cd(Mo_{0.75}W_{0.25})O_4$. Plot b shows also traces of $CdWO_4$ and WO_3.

analysis of the XRD pattern that gives an average value of 1.82 Å in the solid solution (although actually these values fall within the errors).

The IR band near 590 cm^{-1} and the very weak Raman peaks near 550 and 515 cm^{-1} reveal the presence of wolframite impurities, in small amounts in the sample under study. These impurities are in fact revealed also by the Rietveld analysis of the XRD patterns to amount to 1.5% (Figure 6b).

Conclusions

(a) Structural Aspects in the $CdW_{1-x}Mo_xO_4$ System. The present XRD and vibrational study provides further evidence

TABLE 11: Interatomic Distances (Å) and Bond Angles (deg) in Scheelite-Type and Wolframite-Type $CdMo_xW_{1-x}O_4$ Solid Solutions As Determined by the Rietveld Analysis of the Powder XRD Patterns

scheelite-type solid solution polyhedra				wolframite-type solid solution polyhedra			
$(Mo,W)O_4$	Mo,W−O	distances	1.82(2) × 4	$(Mo,W)O_6$	W,Mo−O (I)	distances	1.79(1) × 2
	O−Mo,W−O	angles	115.9(6) × 2		W,Mo−O (II)		1.99(2) × 2
			106.4(7) × 4				2.20(1) × 2
CdO_8	Cd−O	distances	2.38(2) × 4		O(I)-W,Mo−O(I)	angles	101.6(1) × 1
			2.38(1) × 4		O(I)-W,Mo−O(II) sh*		93.0(4) × 2
	O−Cd−O	angles	69.8(5) × 4				104.9(4) × 2
			73.9(5) × 4		O(I)-W,Mo−O(II) l*		86.6(4) × 2
			74.2(5) × 4				168.3(4) × 2
			79.6(5) × 2		sh* O(II)-W,Mo−O(II) sh*		151.7(6) × 1
			99.5(6) × 4		l* O(II)-W,Mo−O(II) l*		86.6(5) × 1
			126.2(5) × 4		l* O(II)-W,Mo−O(II) sh*		82.7(6) × 2
			132.2(5) × 2				76.8(6) × 2
			153.6(5) × 4	CdO_6	Cd−O	distances	2.11(1) × 2
							2.26(1) × 2
							2.42(1) × 2
					O−Cd−O	angles	75.7−161.9

TABLE 12: Spectral Features of Tungsten Species in Different Coordinations

			"terminal" W−O bonds per polyhedron		W−O−W bond lengths	ν(W−O)	ν(W−O−W)
			number	length			
corner-shared distorted octahedra	pseudocubic	WO_3	0		3 × ∼1.8		IR 870, 815, 755, 665
					3 × ∼2.1		R 807, 715
square pyramidal or axially distorted octahedra	tungstite	$WO_3 \times H_2O$	1	1.69	2 × 1.83	IR 948	IR 730, 680
					2 × 1.93	R 948	R 645
edge-shared distorted octahedra	wolframites	$CdWO_4$	2	2 × 1.78	2 × 1.86	IR 884, 835	IR 693, 595
					2 × 2.13	R 896, 771	R 706, 687, 547, 514
isolated tetrahedra	scheelites	$CaWO_4$	4	4 × 1.79		IR 813	
						R 910, 836, 795	
	spinels	Na_2WO_4	4			IR 840	
						R 930, 814	
	ion in water		4			IR 833	
						R 931, 833	
isolated nearly symmetrical octahedra	ordered perovskites	Ba_2CaWO_6	6	6 × ∼1.8		IR 620	
						R 818	

for the limited reciprocal solubility of scheelite-type $CdMoO_4$ and wolframite-type $CdWO_4$. The bond length and bond angles deduced from the Rietveld analysis of the experimental XRD patterns suggest that critical factors to determine the phase transition can be associated with the forced contraction of the CdO_6 octahedra in the scheelite structure of $CdWO_4$, further forced to contract by Mo addition. These data agree with the possibility of converting scheelites into wolframites by compression.[1,14,15]

(b) Interpretation of the Vibrational Spectra of Wolframite-Type $CdWO_4$. The model we adopted gives rise to a quite satisfactory interpretation of the vibrational spectra of $CdWO_4$. It is concluded that an interpretation of these spectra based on a tetrahedral coordination of tungsten, as proposed by Blasse,[12] is unsatisfactory, because it does not justify the presence of the Raman peaks in the region 600−500 cm^{-1}, which are in fact due to the symmetric stretchings of the very asymmetric W−O−W bonds, which are "dissected" or neglected if tetrahedra are supposed to exist. This is a quite interesting result in view of the use of vibrational spectroscopies to determine the coordination of W and/or Mo compounds with unknown structure. Octahedral-versus-tetrahedral coordination can be determined better in the medium region of the IR range, where the vibrations associated with bridging oxygen are observable, than in the higher frequency region, where stretching of the "terminal" W,Mo−O bonds can be found.

The interpretation given here is more detailed than that recently given for wolframite-like mixed tungstates by Hanuza et al.,[13] allowing the distinction between vibrations of terminal W−O bonds and of W−O−W bridges.

(c) Interpretation of the Vibrational Spectra of $CdW_{1-x}Mo_xO_4$ Solid Solutions. The Raman spectra of both the scheelite-type and the wolframite-type $CdW_{1-x}Mo_xO_4$ solid solutions show that higher frequency peaks (associated with the stretchings of Mo,W−O bonds) split. In parallel, the corresponding IR spectra show that the prominent IR bands at high frequency shift. The new components are mostly, but not totally, associated with higher frequencies for W−O bonds with respect to Mo−O bonds. The apparently different behavior of the Raman peaks and IR bands is likely simply associated with their bandwidth, which is sharper in Raman and broader in IR, due to the fact that the "polar" modes (i.e. those active in IR) give rise to transverse-longitudinal (TO-LO) splittings. In the case of powder IR spectra, this results in a dependence of the peak position on particle morphologies and in a definite band broadening, because of the averaging of the IR spectra of particles with different morphologies.[31]

In any case, the sensitivity of the W,Mo−O stretching modes to Mo or tungsten substitution is indicative of the "localized" character of these modes. In contrast, IR and Raman peaks at lower frequencies, mainly associated with deformation modes and lattice vibrations, seem to be unaffected by Mo for W substitution. This points to a "framework" character of such modes.

In the case of wolframite-type solid solutions, both IR and Raman spectra show that Mo for W substitution affects significantly the bond strength; that is, the terminal Mo−O bonds are weaker than the W−O bonds. In the case of the scheelite-type solid solutions, instead, it appears that the internal

couplings of modes of the tetrahedra are also affected, possibly due to relevant changes in the O−M−O bond angles.

(d) The Correlation of M−O Stretching Force Constant versus Bond Length and the "Diatomic Approximation Approach" to the Vibrational Spectra of Molybdates and Tungstates. As already cited, Cotton and Wing[24] first reported a correlation between M−O stretching force constant k and bond lengths, r, in molybdate compounds. Daniel et al.[23] concluded that the same correlation curve is also valid for tungstates. In Figure 5 we reported the points of molybdates and tungstates of both authors. We added on the same curve also the points relative to Cd molybdate and Cd tungstate, based on the results presented here, that also roughly agree with the correlation. The points are better fitted by the exponential curves

$$k = 1817.91\mathrm{e}^{-3.21403r} \qquad \text{for tungstates}$$

$$k = 3407.23\mathrm{e}^{-3.63657r} \qquad \text{for molybdates}$$

Recently, Hardcastle and Wachs proposed an approximated method, called the "diatomic approximation approach", for the interpretation of the Raman spectra of molybdates[32] and vanadates.[33] They cited that a similar correlation can be done for tungstates.[16,33] These authors proposed that the Raman spectra of molybdates can be interpreted assuming that each Mo−O bond behaves as an independent vibrator and gives rise to Raman active stretching bands whose frequency ν is related to the Mo−O distance $r_{\mathrm{Mo-O}}$ through the following empirical relation:

$$r_{\mathrm{Mo-O}} = 0.48239 \ln(32895/\nu)$$

According to the expression relating the force constant to the wavenumber for single, terminal Mo−O bonds,[23] $\nu^2 = 1.23833 \times 10^5 k$, the curve of Hardcastle and Wachs can be transformed into the following:

$$k = 8738.22\mathrm{e}^{-4.1460r}$$

This curve is plotted in Figure 5 and also appears to fit quite satisfactorily the data. However, it is clear that the "diatomic approximation approach" proposed by Hardcastle and Wachs is based on very coarse hypotheses. These authors completely neglect both intramolecular couplings (when terminal MoO_x groups occur, with $x > 1$) and intermolecular couplings (when more than one molecular unit is present in the smallest Bravais cell). They only use Raman peaks, completely neglecting the IR active modes. This can be partially successful only when the smallest Bravais cell contains two molybdate species. In fact, only in this case (and if the unit cell is centrosymmetric and no silent modes occur) can the number of Raman active stretching modes correspond to the number of Mo−O bonds. As an example, this in not the case of the isostructural vanadates $Mg_3(VO_4)_2$, studied by some of us,[34] and $Zn_3(VO_4)_2$, studied by Hardcastle and Wachs,[33] where $Z = 4$; in these cases the number of Raman active stretching modes exceeds that of equivalent V−O bonds.

The hypothesis of Hardcastle and Wachs,[32,33] with no need of calculating the stretching force constant, allows very simple evaluations of the metal−oxygen bond lengths, but the errors arising from these calculations can be quite high, certainly greater than those obtained by previous calculation of the force constant. Moreover, the determination of the number of different Mo−O bonds is complex. The application of the Hardcastle and Wachs's equation to the Raman peaks of $CdMoO_4$ (863, 822, and 759 cm^{-1}) allows the calculation of Mo−O distances of 1.7562, 17797, and 1.8182 Å, while by using the simplified equations given by Cotton and Wing[24] and the above fitting equation, we calculate a bond length of 1.780 Å. According to the Rietveld analysis of the XRD pattern, the four Mo−O bonds are all equivalently long, 1.75(1) Å.

SCHEME 1: Structures for Tungstate Species as the Models for the Surface Species on Metal Oxide Carriers

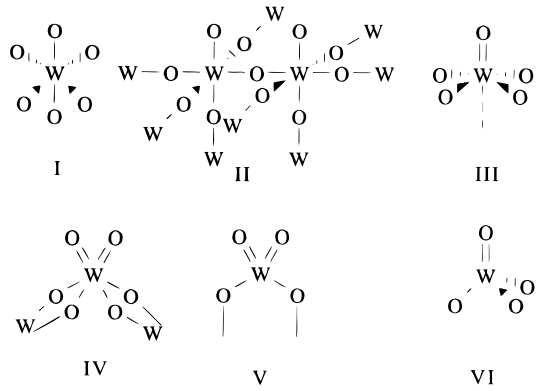

(e) On the Structure of Tungsten Oxide Species in Supported Metal Oxide "Monolayers". The interpretation of the Raman and IR spectra is the key to propose surface structures for the active sites of metal oxide-supported WO_3 heterogeneous catalysts. This interpretation is usually based on the comparison of their vibrational spectra with those of model bulk compounds. For tungsten-oxide "monolayer" species the identification of the structure is usually done assuming alternative "tetrahedral" or "octahedral" coordination for tungsten.[35,36] However, looking at the structures taken by tungstate species (Table 12), it seems clear that this view is oversimplified. Coordination of W^{6+} cannot frequently be described as "tetrahedral" or "octahedral", and the vibrational spectra depend more on the number of short and long bonds than on the overall 4-fold, 5-fold, or 6-fold coordination, frequently highly distorted.

This question appies, in particular, to the so-called "octahedral tungstate species". In fact WO_6 octahedra can be "isolated" (as in the perovskite Ba_2CaWO_6,[37] with all W−O bonds assumed to be "terminal" and nearly equivalent, structure I), corner sharing (as in pseudocubic WO_3, with all oxygens bridging between two W ions, structure II), and axially distorted giving rise to near a square pyramid with one short W═O bond (as in the case of the compound $WO_3 \times H_2O$[24] and of polyoxotungstates[38] and of wolframyl complexes,[23,38] structure III). Finally, the wolframite-type compounds like $CdWO_4$ can be taken as a model for "octahedrally coordinated" polymeric tungstate species with two "terminal" W−O bonds, i.e. of dioxotungsten oxide species (structure IV).

On oxide-supported WO_3 catalysts, at low surface coverages the predominant species is characterized by a peak in both IR and Raman spectra located in the range 1000−950 cm^{-1} on wet surfaces and at 1025−1000 cm^{-1} on dry surfaces.[35,36,39−42] Only at quite high coverages do other bands appear in both IR and Raman spectra, at lower frequencies. This peak is quite unanimously referred to as an isolated "mononuclear" WO_y species. In the literature, the species responsible for these spectral features has been frequently "modeled" as a dioxo species,[39,43−45] represented as structure V in Scheme 1. However, this species has been alternatively identified, for several years,[46] as a mono-oxo wolframyl species, i.e. a species with a single W═O double bond, similar to structure III. This assignment is based, among other reasons, on the fact that the same peak position is found in IR and Raman spectra. As we previously stated, this cannot occur with dioxo species, where ν_{sym}(W═O) and ν_{as}(W═O) must be split and must have different

intensity ratios in IR and Raman spectra. Accordingly, the spectra of $CdWO_4$, where the coordination at tungsten (structure IV) is "dioxo", similar to that proposed in the literature for such surface wolframate species, confirm our previous statement.

Incidentally, we disagree also with the description of the most evident species in oxide-supported WO_3 as "distorted tetrahedral", done by several authors that agree with the mono-oxo nature of these species[35,36] but suggest the structure VI. In fact, tetrahedral species, like those formed in scheelites, are characterized by four nearly equivalent bonds and give rise to one to four Raman active stretching bonds depending on their overall symmetry. In the case of such surface species, instead, one bond is definitely shorter than the others. We had proposed some years ago[40,41] to describe this surface species as a "wolframyl" species, being, among other things, unclear how many longer W−O bonds are also present (with a possibly difference in the cases of wet and dry surfaces).

In any case, the spectral study of wolframite and scheelite-like structure discussed here allows a model of a "dioxo" species and of the true "tetrahedral" species and further supports the previous identification of the surface species on WO_3-TiO_2 and $WO_3-Al_2O_3$ catalysts as a species different from both, i.e. a "mono-oxo" wolframyl pyramidal species.

Acknowledgment. This work has been supported, in part, by MURST, Rome, Italy. M.D. acknowledges Prof. B. Raveau for encouragement and helpful discussions and for the hospitality in his laboratory.

References and Notes

(1) Sleight, A. W. *Acta Crystallogr. B* **1972**, *28*, 2899.
(2) Fagherazzi, G.; Pernicone, N. *J. Catal.* **1970**, *16*, 321.
(3) Moro-Oka, Y.; Ueda, W. *Advances in Catalysis*; Eley, D. D., Pines, H., Haag, W. O., Eds.; Academic Press: New York, 1994; Vol. 40, p 233.
(4) Hyde, B. G.; Andersson, S. *Inorganic Crystal Structure*; Wiley: New York, 1989.
(5) Zhuravlev, V. D.; Khodos, M. Ya.; Velikodnyi, Yu. A. *Russ. J. Inorg. Chem.* **1994**, *39*, 464.
(6) Tarte, P.; Liegeois-Duyckaerts, N. *Spectrochim. Acta, Part A* **1972**, *28*, 2029.
(7) Liegeois-Duyckaerts, N.; Tarte, P. *Spectrochim. Acta, Part A* **1972**, *28*, 2037.
(8) Barker, A. S. *Phys. Rev. A* **1964**, *135*, 742.
(9) Khanna, R. K.; Lippincott, E. R. *Spectrochim. Acta, Part A* **1968**, *24*, 905.
(10) Brown, R. G.; Denning, J.; Hallett, A.; Ross, S. D. *Spectrochim. Acta, Part A* **1970**, *26*, 963.
(11) Cord, P. P.; Courtine, P.; Pannetier, G.; Guillermet, J. *Spectrochim. Acta, Part A* **1972**, *28*, 1601.
(12) Blasse, G. *J. Inorg. Nucl. Chem.* **1975**, *37*, 97.
(13) Hanuza, J.; Maczka, M.; van der Maas, J. H. *J. Solid State Chem.* **1995**, *117*, 177.
(14) Jayaraman, A.; Batlogg, B.; van Uitert, L. G. *Phys. Rev. B* **1983**, *28*, 4774.
(15) Jayaraman, A.; Wang, S. Y. Sharma, S. K. *Curr. Science* **1995**, *69*, 44.
(16) Wachs, I. E. *Catal. Today* **1996**, *27*, 437.
(17) Daturi, M.; Borel, M. M.; Leclaire, A.; Savary, L.; Costentin, G.; Lavalley, J. C.; Raveau, B. *J. Chim. Phys.* **1996**, *93*, 2043.
(18) Rodriguez-Carvajal, Laboratoire Léon Brillouin, Saclay, Oct. 1994.
(19) Macavei, J.; Schulz, H. *Z. Kristallogr.* **1993**, *207*, 193.
(20) Chicjagov, A. V.; Dem'yanets, L. N.; Ilyukhin, V. V.; Belov, N. V. *Kristallografija* **1966**, *11*, 686.
(21) Fateley, W. G.; Dollish, F. R.; McDevitt, N. T.; Bentley, F. F. *Infrared and Raman Selection Rules for Molecular and Lattice Vibrations: the Correlation Method*; Wiley: New York, 1972.
(22) Moeller, T. *Inorganic Chemistry*; Wiley: New York, 1982.
(23) Daniel, M. F.; Desbat, B.; Lassegues, J. C.; Gerand, B.; Figlarz, M. *J. Solid State Chem.* **1987**, *67*, 235.
(24) Cotton, F. A.; Wing, R. M. *Inorg. Chem.* **1965**, *4*, 867.
(25) Shannon, R. D. *Acta Crystallogr., Sect. A* **1976**, *32*, 751.
(26) Shannon, R. D.; Prewitt, C. T. *Acta Crystallogr., Sect. B* **1969**, *25*, 925.
(27) Busey, R. H.; Keller, O. L. *J. Chem. Phys.* **1964**, *44*, 215.
(28) Busca, G.; Lavalley, J. C. *Spectrochim. Acta, Part A* **1986**, *42*, 443.
(29) Baraton, M. I.; Busca, G.; Prieto, M. C.; Ricchiardi, G.; Sanchez Escribano, V. *J. Solid State Chem.* **1994**, *112*, 9.
(30) Busca, G.; Buscaglia, V.; Leoni, M.; Nanni, P. *Chem. Mater.* **1994**, *6*, 955.
(31) Hadni, A. In *The Infrared Spectra of Minerals*; Farmer, V. C., Ed.; The Mineralogical Society: London, 1974; p 27.
(32) Hardcastle, F. D.; Wachs, I. E. *J. Phys. Chem.* **1991**, *95*, 10763.
(33) Hardcastle, F. D.; Wachs, I. E. *J. Phys. Chem.* **1991**, *95*, 5031.
(34) Busca, G.; Ricchiardi, D.; Sam, S. H.; Volta, J. C. *J. Chem. Soc., Faraday Trans.* **1994**, *90*, 1161.
(35) Kim, D. S.; Ostromecki, M.; Wachs, I. E. *J. Mol. Catal. A: Chem.* **1996**, *106*, 93.
(36) Horsley, J. A.; Wachs, I. E.; Brown, J. M.; Via, G. H.; Hardcastle, F. D. *J. Phys. Chem.* **1987**, *91*, 4014.
(37) Blasse, G.; Corsmit, F. *J. Solid State Chem.* **1973**, *6*, 513.
(38) Cotton, F. A.; Wilkinson, G. *Advanced Inorganic Chemistry*, 4th ed.; Wiley: New York, 1980.
(39) Soled, S. L.; McVicker, G. B.; Murrell, L. L.; Sherman, L. G.; Dispenziere, N. C.; Hsu, S. L.; Waldman, D. *J. Catal.* **1988**, *111*, 286.
(40) Busca, G.; Lavalley, J. C. *Spectrochim. Acta, Part A* **1986**, *42*, 443.
(41) Ramis, G.; Busca, G.; Cristiani, C.; Lietti, L.; Forzatti, P.; Bregani, F. *Langmuir* **1992**, *8*, 1744.
(42) Alemany, L. J.; Lietti, L.; Ferlazzo, N.; Forzatti, P.; Busca, G.; Giamello, E.; Bregani, F. *J. Catal.* **1995**, *155*, 117.
(43) Bond, G. C.; Flamerz, S.; van Wijk, L. *Catal. Today* 1987, *1*, 229.
(44) Arata, K.; Hino, M. In *Proc. 9th ICC*, Calgary, 1988; p 1727.
(45) Vermaire, D. C.; vanBerge, P. C. *J. Catal.* **1989**, *116*, 309.
(46) Hilbzig, F.; Gobel, H. E.; Knözinger, H.; Schmelz, H.; Leugeler, B. *J. Phys. Chem.* **1991**, *95*, 6974.